

Waypoint guidance control for underwater snake robots exposed to ocean currents

E. Kelasidi, A. M. Kohl, K. Y. Pettersen and J. T. Gravdahl

Abstract—This paper presents a waypoint guidance strategy for underwater snake robots, which is an extension of the straight line path following controllers previously proposed by the authors. The proposed waypoint guidance control enables an underwater snake robot to converge towards and follow a desired path compensating for disturbances due to ocean currents effects. The ocean currents are constant and irrotational, and with unknown magnitude and direction. A set of waypoints is chosen along the desired path which is then defined by interconnecting these waypoints by straight lines. Simulation results for both lateral undulation and eel-like motion illustrate the performance of the guidance strategy.

I. INTRODUCTION

In today's subsea operations like exploration, and inspection and maintenance of offshore structures for example in the oil and gas industry, there is a large potential for improving efficiency and reducing costs by increasing the autonomy. This requires the development of new systems that are more robust, agile, and versatile than existing technology. A large variety of species that have adapted to subsea conditions and that are specialised in propelling and maneuvering underwater can be found in nature. Bio-inspired robots that mimic the motion of eels, also referred to as underwater snake robots (USRs), are therefore considered promising to provide solutions for improved autonomy in the future.

Several prototypes of such bio-inspired robots have been developed [1], [2], [3], and also their mathematical modelling has been addressed widely in the literature [4], [5], [6], [7], [8]. In order to be able to operate autonomously, however, the development of efficient guidance algorithms for USRs is a prerequisite. In [9], a control system was developed which enabled an eel-like robot to follow a straight line. The authors of [10] proposed a virtual-target guidance law for path-following of an eel-like robot, and in [11], trajectory tracking of a fish robot was developed. However, neither of the above works consider the disturbance from ocean currents. A popular guidance strategy for marine systems, that extends straight line path-following, is waypoint guidance (WPG) [12]. For land-based snake robots, WPG was proposed in [13]. WPG can also be applied for underwater bio-mimetic

robots: A control system for a three-linked robotic fish was developed in [14], and in [15] WPG was applied to achieve obstacle avoidance of a USR. Both cases did not consider ocean currents. Experimental results of a fish robot tracking a closed trajectory in the presence of a current were presented in [16]. However, no theoretical analysis of the control system was provided. To the authors' best knowledge, waypoint guidance control for steering a USR between arbitrary locations in a plane has not been employed previously for path following control of underwater snake robots exposed to currents.

The main contribution of this paper compared to the previous work presented in [15] is the compensation for the disturbances due to the constant irrotational current effects of unknown direction and magnitude. A waypoint guidance strategy is proposed for steering an underwater snake robot compensating for the current effects along a desired path defined by a set of waypoints interconnected by straight lines. Hence, this paper extends the waypoint guidance presented in [15] by considering the current effects and thus the control approach presented in [15] falls out as a special case where the current effects are neglected. In addition, the proposed guidance strategy in this paper can be combined with two different straight line path following control approaches previously proposed by the authors in [17], [18] and [19]. An integral line-of-sight (ILOS) path following controller derived based on the model proposed in [4] for USRs for which the stability analysis was studied using a Poincaré map was presented and experimentally validated in [18] and [19]. In [17], a path following controller was proposed based on a control-oriented, simplified model, and a general formal stability proof was presented for the closed-loop system. This paper extends the previous work by the authors on ILOS path following along straight lines presented in [17], [18] and [19], proposing an operator-friendly framework for waypoint guidance control of USRs under the influence of ocean current effects. Simulation results are presented for both lateral undulation and eel-like motion patterns illustrating the performance of the proposed waypoint guidance strategy. In particular, the simulation results show that the waypoint guidance control strategy presented in this paper can be applied to USRs to compensate for the ocean current effect and achieve path following along interconnected straight lines independently of the underlying model and heading control system.

The paper is organized as follows. Section II and Section III present a complex model and a control-oriented model of a USR, respectively. The ILOS path following control

E. Kelasidi, A. M. Kohl and K. Y. Pettersen are with the Centre for Autonomous Marine Operations and Systems, Dept. of Engineering Cybernetics at NTNU, NO-7491 Trondheim, Norway. E-mail: {Eleni.Kelasidi,Anna.Kohl,Kristin.Y.Pettersen}@itk.ntnu.no

J. T. Gravdahl is with the Dept. of Engineering Cybernetics at NTNU, NO-7491 Trondheim, Norway. E-mail: Tommy.Gravdahl@itk.ntnu.no

Research partly funded by VISTA a basic research program in collaboration between The Norwegian Academy of Science and Letters, and Statoil, and partly supported by the Research Council of Norway through its Centres of Excellence funding scheme, project no. 223254-NTNU AMOS.

approaches along straight lines are presented in Section IV, while the waypoint guidance strategy for USRs under the influence of ocean current effects is outlined in Section V. Simulation results are presented for both lateral undulation and eel-like motion patterns in Section VI, followed by conclusions and suggestions for further research in Section VII.

II. COMPLEX MODEL OF UNDERWATER SNAKE ROBOT

This section briefly presents the model of the kinematics and dynamics of an underwater snake robot moving in a virtual horizontal plane previously presented in [4], [18], for completeness of the paper. This model will be used to simulate the behavior of an underwater snake robot in Section VI.

A. Notations and Defined Symbols

The underwater snake robot consists of n rigid links of equal length $2l$ interconnected by $n-1$ joints. The links are assumed to have the same mass m and moment of inertia $J = \frac{1}{3}ml^2$. The mass of each link is uniformly distributed so that the link CM (center of mass) is located at its center point (at length l from each side). The total mass of the robot is therefore nm . The following vectors and matrices are used in the subsequent sections:

$$\mathbf{A} = \begin{bmatrix} 1 & 1 & & \\ & \ddots & \ddots & \\ & & 1 & 1 \\ & & & & 1 & -1 \end{bmatrix}, \mathbf{D} = \begin{bmatrix} 1 & -1 & & \\ & \ddots & \ddots & \\ & & 1 & -1 \end{bmatrix},$$

where $\mathbf{A}, \mathbf{D} \in \mathbb{R}^{(n-1) \times n}$. Furthermore, $\bar{\mathbf{D}} = \mathbf{D}^T (\mathbf{D}\mathbf{D}^T)^{-1}$,

$$\mathbf{e} = [1, \dots, 1]^T \in \mathbb{R}^n, \mathbf{E} = \begin{bmatrix} \mathbf{e} & \mathbf{0}_{n \times 1} \\ \mathbf{0}_{n \times 1} & \mathbf{e} \end{bmatrix} \in \mathbb{R}^{2n \times 2},$$

$$\mathbf{S}_\theta = \text{diag}(\sin \theta) \in \mathbb{R}^{n \times n}, \quad \mathbf{C}_\theta = \text{diag}(\cos \theta) \in \mathbb{R}^{n \times n}$$

$$\dot{\theta}^2 = [\dot{\theta}_1^2, \dots, \dot{\theta}_n^2]^T \in \mathbb{R}^n, \mathbf{K} = \mathbf{A}^T (\mathbf{D}\mathbf{D}^T)^{-1} \mathbf{D}$$

B. Kinematics of Underwater Snake Robot

The snake robot is assumed to move in a virtual horizontal plane, fully immersed in water, and has $n+2$ degrees of freedom (n links angles and the x - y position of the robot). The *link angle* of each link $i \in 1, \dots, n$ of the snake robot is denoted by $\theta_i \in \mathbb{R}$, while the *joint angle* of joint $i \in 1, \dots, n-1$ is given by $\phi_i = \theta_i - \theta_{i+1}$. The link angles and the joint angles are assembled in the vectors $\boldsymbol{\theta} = [\theta_1, \dots, \theta_n]^T \in \mathbb{R}^n$ and $\boldsymbol{\phi} = [\phi_1, \dots, \phi_{n-1}]^T \in \mathbb{R}^{n-1}$, respectively. The *heading* (or *orientation*) $\bar{\theta} \in \mathbb{R}$ of the snake is defined as the average of the link angles [13], i.e. as

$$\bar{\theta} = \frac{1}{n} \sum_{i=1}^n \theta_i. \quad (1)$$

The global frame position $\mathbf{p}_{\text{CM}} \in \mathbb{R}^2$ of the CM of the robot is given by

$$\mathbf{p}_{\text{CM}} = \begin{bmatrix} p_x \\ p_y \end{bmatrix} = \begin{bmatrix} \frac{1}{nm} \sum_{i=1}^n m x_i \\ \frac{1}{nm} \sum_{i=1}^n m y_i \end{bmatrix} = \frac{1}{n} \begin{bmatrix} \mathbf{e}^T \mathbf{X} \\ \mathbf{e}^T \mathbf{Y} \end{bmatrix}, \quad (2)$$

where (x_i, y_i) are the global frame coordinates of the CM of link i , $\mathbf{X} = [x_1, \dots, x_n]^T \in \mathbb{R}^n$ and $\mathbf{Y} = [y_1, \dots, y_n]^T \in \mathbb{R}^n$.

C. Hydrodynamic Modeling

Regarding the hydrodynamic model, in [4] it is shown that the fluid forces on all links can be expressed in vector form as

$$\mathbf{f} = \begin{bmatrix} \mathbf{f}_x \\ \mathbf{f}_y \end{bmatrix} = \begin{bmatrix} \mathbf{f}_{\text{Ax}} \\ \mathbf{f}_{\text{Ay}} \end{bmatrix} + \begin{bmatrix} \mathbf{f}_{\text{Dx}}^I \\ \mathbf{f}_{\text{Dy}}^I \end{bmatrix} + \begin{bmatrix} \mathbf{f}_{\text{Dx}}^{II} \\ \mathbf{f}_{\text{Dy}}^{II} \end{bmatrix}. \quad (3)$$

The vectors \mathbf{f}_{Ax} and \mathbf{f}_{Ay} represent the effects from added mass forces and are expressed as

$$\begin{bmatrix} \mathbf{f}_{\text{Ax}} \\ \mathbf{f}_{\text{Ay}} \end{bmatrix} = - \begin{bmatrix} \mu_n (\mathbf{S}_\theta)^2 & -\mu_n \mathbf{S}_\theta \mathbf{C}_\theta \\ -\mu_n \mathbf{S}_\theta \mathbf{C}_\theta & \mu_n (\mathbf{C}_\theta)^2 \end{bmatrix} \begin{bmatrix} \ddot{\mathbf{X}} \\ \ddot{\mathbf{Y}} \end{bmatrix} - \begin{bmatrix} -\mu_n \mathbf{S}_\theta \mathbf{C}_\theta & -\mu_n (\mathbf{S}_\theta)^2 \\ \mu_n (\mathbf{C}_\theta)^2 & \mu_n \mathbf{S}_\theta \mathbf{C}_\theta \end{bmatrix} \begin{bmatrix} \mathbf{V}_x^a \\ \mathbf{V}_y^a \end{bmatrix} \dot{\boldsymbol{\theta}}, \quad (4)$$

where $\mathbf{V}_x^a = \text{diag}(V_{x,1}, \dots, V_{x,n}) \in \mathbb{R}^{n \times n}$, $\mathbf{V}_y^a = \text{diag}(V_{y,1}, \dots, V_{y,n}) \in \mathbb{R}^{n \times n}$ and $[V_{x,i}, V_{y,i}]^T$ is the current velocity expressed in inertial frame coordinates. The drag forces on the robot are given by

$$\begin{bmatrix} \mathbf{f}_{\text{Dx}}^I \\ \mathbf{f}_{\text{Dy}}^I \end{bmatrix} = - \begin{bmatrix} c_t \mathbf{C}_\theta & -c_n \mathbf{S}_\theta \\ c_t \mathbf{S}_\theta & c_n \mathbf{C}_\theta \end{bmatrix} \begin{bmatrix} \mathbf{V}_{\text{rx}} \\ \mathbf{V}_{\text{ry}} \end{bmatrix}, \quad (5)$$

$$\begin{bmatrix} \mathbf{f}_{\text{Dx}}^{II} \\ \mathbf{f}_{\text{Dy}}^{II} \end{bmatrix} = - \begin{bmatrix} c_t \mathbf{C}_\theta & -c_n \mathbf{S}_\theta \\ c_t \mathbf{S}_\theta & c_n \mathbf{C}_\theta \end{bmatrix} \text{sgn} \left(\begin{bmatrix} \mathbf{V}_{\text{rx}} \\ \mathbf{V}_{\text{ry}} \end{bmatrix} \right) \begin{bmatrix} \mathbf{V}_{\text{rx}}^2 \\ \mathbf{V}_{\text{ry}}^2 \end{bmatrix}, \quad (6)$$

where $\mathbf{f}_{\text{Dx}}^I, \mathbf{f}_{\text{Dy}}^I$ and $\mathbf{f}_{\text{Dx}}^{II}, \mathbf{f}_{\text{Dy}}^{II}$ represent the effects from the linear and nonlinear drag forces, respectively, and where the relative velocities are given by

$$\begin{bmatrix} \mathbf{V}_{\text{rx}} \\ \mathbf{V}_{\text{ry}} \end{bmatrix} = \begin{bmatrix} \mathbf{C}_\theta & \mathbf{S}_\theta \\ -\mathbf{S}_\theta & \mathbf{C}_\theta \end{bmatrix} \begin{bmatrix} \dot{\mathbf{X}} - \mathbf{V}_x \\ \dot{\mathbf{Y}} - \mathbf{V}_y \end{bmatrix}. \quad (7)$$

In addition, the fluid torques on all links are

$$\tau = -\Lambda_1 \dot{\theta} - \Lambda_2 \dot{\theta} - \Lambda_3 \dot{\theta} |\dot{\theta}|, \quad (8)$$

where $\Lambda_1 = \lambda_1 \mathbf{I}_n$, $\Lambda_2 = \lambda_2 \mathbf{I}_n$ and $\Lambda_3 = \lambda_3 \mathbf{I}_n$. The coefficients $c_t, c_n, \lambda_2, \lambda_3$ represent the drag parameters due to the pressure difference between the two sides of the body, and the parameters μ_n, λ_1 represent the added mass of the fluid carried by the moving body.

D. Equations of Motion

This section presents the equations of motion for the underwater snake robot. In [4], [18] it is shown that the acceleration of the CM may be expressed as

$$\begin{bmatrix} \ddot{p}_x \\ \ddot{p}_y \end{bmatrix} = -\mathbf{M}_p \begin{bmatrix} \mathbf{k}_{11} & \mathbf{k}_{12} \\ \mathbf{k}_{21} & \mathbf{k}_{22} \end{bmatrix} \begin{bmatrix} l \mathbf{K}^T (\mathbf{C}_\theta \dot{\theta}^2 + \mathbf{S}_\theta \ddot{\boldsymbol{\theta}}) \\ l \mathbf{K}^T (\mathbf{S}_\theta \dot{\theta}^2 - \mathbf{C}_\theta \ddot{\boldsymbol{\theta}}) \end{bmatrix} - \mathbf{M}_p \begin{bmatrix} \mathbf{k}_{12} & -\mathbf{k}_{11} \\ \mathbf{k}_{22} & -\mathbf{k}_{21} \end{bmatrix} \begin{bmatrix} \mathbf{V}_x^a \\ \mathbf{V}_y^a \end{bmatrix} \dot{\boldsymbol{\theta}} + \mathbf{M}_p \begin{bmatrix} \mathbf{e}^T \mathbf{f}_{\text{Dx}} \\ \mathbf{e}^T \mathbf{f}_{\text{Dy}} \end{bmatrix}, \quad (9)$$

where the detailed derivation of the matrix \mathbf{M}_p and vectors $\mathbf{k}_{11}, \mathbf{k}_{12}, \mathbf{k}_{21}$ and \mathbf{k}_{22} is given in [4], [18]. In addition, it is shown that under the influence of fluid forces (3) and torques (8), the complete equation of motion of the underwater snake robot are obtained by (9) and

$$\mathbf{M}_\theta \ddot{\boldsymbol{\theta}} + \mathbf{W}_\theta \dot{\boldsymbol{\theta}}^2 + \mathbf{V}_\theta \dot{\boldsymbol{\theta}} + \Lambda_3 |\dot{\boldsymbol{\theta}}| \dot{\boldsymbol{\theta}} + \mathbf{K}_{\text{Dx}} \mathbf{f}_{\text{Dx}} + \mathbf{K}_{\text{Dy}} \mathbf{f}_{\text{Dy}} = \mathbf{D}^T \bar{\mathbf{u}}, \quad (10)$$

with $\mathbf{f}_{\text{Dx}} = \mathbf{f}_{\text{Dx}}^I + \mathbf{f}_{\text{Dx}}^{II}$ and $\mathbf{f}_{\text{Dy}} = \mathbf{f}_{\text{Dy}}^I + \mathbf{f}_{\text{Dy}}^{II}$ representing the drag forces in x and y direction and $\bar{\mathbf{u}} \in \mathbb{R}^{n-1}$ the control input. For more details and the derivation of the matrices $\mathbf{M}_\theta, \mathbf{W}_\theta, \mathbf{V}_\theta, \mathbf{K}_{\text{Dx}}$ and \mathbf{K}_{Dy} , see [18].

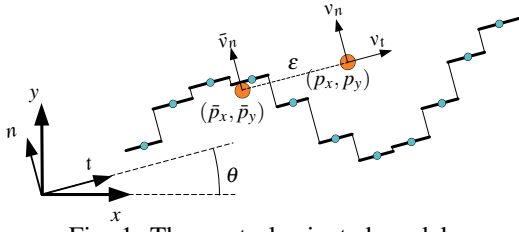


Fig. 1: The control-oriented model

III. CONTROL-ORIENTED MODEL OF UNDERWATER SNAKE ROBOT

In this section, a simplified modelling approach for USRs is introduced briefly and a transformation to make it suitable for path-following is presented. A detailed derivation of the model can be found in [20], [21], an analysis and comparison with the complex model from the previous section in [8], and the model transformation in [17].

A. Equations of motion

The control-oriented model requires that the USR moves slowly with a sinusoidal gait, such as lateral undulation or eel-like motion. The key assumption for the modelling is that the overall behaviour of the USR can be captured by looking at the link translation relative to the direction of forward motion. This assumption is based on the observation that during a sinusoidal gait with limited link angles, the rotational motion of each link can be approximated by a translational displacement of the CM of each link, and that it is this displacement that creates the forces pushing the USR forward. For the description of the USR, two coordinate frames are introduced: the global x - y -frame, and the body-aligned t - n -frame. The geometry and different coordinate frames of the model can be seen in Fig. 1.

The length of each link is now $L = 2l$, and the single links are now interconnected by $n - 1$ prismatic joints. The $n + 2$ degrees of freedom of the control-oriented model correspond to the position in the plane (p_x, p_y) , the $n - 1$ joint coordinates ϕ_i , and the orientation θ . Note that by this approach, all links have the same orientation, which also defines the orientation of the robot. With a linearising feedback law, the joint coordinates ϕ_i are directly controlled by the input $\bar{u} \in \mathbb{R}^{N-1}$, details on the controller can be found in [8]. The dynamical equations of the control-oriented model are:

$$\dot{\phi} = v_\phi, \quad (11a)$$

$$\dot{\theta} = v_\theta, \quad (11b)$$

$$\dot{p}_x = v_t \cos \theta - v_n \sin \theta, \quad (11c)$$

$$\dot{p}_y = v_t \sin \theta + v_n \cos \theta, \quad (11d)$$

$$\dot{v}_\phi = \bar{u}, \quad (11e)$$

$$\dot{v}_\theta = -\tilde{\lambda}_1 v_\theta + \frac{\tilde{\lambda}_2}{n-1} v_{t,\text{rel}} \bar{e}^T \phi, \quad (11f)$$

$$\dot{v}_t = -\frac{c_t}{m} v_{t,\text{rel}} + \frac{2c_p}{nm} \bar{e}^T \phi v_{n,\text{rel}} - \frac{c_p}{nm} \phi^T A \bar{D} v_\phi, \quad (11g)$$

$$\dot{v}_n = \frac{2c_p}{nm} \bar{e}^T \phi v_{t,\text{rel}} - \frac{c_n}{m} v_{n,\text{rel}}. \quad (11h)$$

The parameters $\tilde{\lambda}_i$ are empirical constants determining the rotational dynamics, and the parameter c_p is the propulsion

coefficient. The variables $v_{n,\text{rel}}, v_{t,\text{rel}}$ represent the relative velocity in normal and tangential direction, respectively.

B. Model transformation

In order to make the model (11) more suitable for control-design, the point that defines the position of the robot was moved to the pivot point, about which the USR turns in [17]: In the dynamical equations (11f) and (11h) it can be seen that the joint coordinates ϕ enter the dynamics of both v_n and v_θ . This can be avoided by moving the point that defines the position of the snake robot by a distance ϵ in the tangential direction, as can be seen in Fig. 1. The coefficient $\epsilon = -\frac{2(n-1)c_p}{nm\tilde{\lambda}_2}$ is obtained from (11f) and (11h). The new coordinates are then defined as

$$\bar{p}_x = p_x + \epsilon \cos \theta, \quad (12a)$$

$$\bar{p}_y = p_y + \epsilon \sin \theta, \quad (12b)$$

$$\bar{v}_n = v_n + \epsilon v_\theta. \quad (12c)$$

With the transformation (12b), (12c), the model written in the new coordinates is

$$\dot{\phi} = v_\phi, \quad (13a)$$

$$\dot{\theta} = v_\theta, \quad (13b)$$

$$\dot{\bar{p}}_y = v_{t,\text{rel}} \sin \theta + \bar{v}_{n,\text{rel}} \cos \theta + V_y, \quad (13c)$$

$$\dot{v}_\phi = \bar{u}, \quad (13d)$$

$$\dot{v}_\theta = -\lambda_1 v_\theta + \frac{\lambda_2}{n-1} v_{t,\text{rel}} \bar{e}^T \phi, \quad (13e)$$

$$\dot{\bar{v}}_{n,\text{rel}} = (X + V_t) v_\theta + Y \bar{v}_{n,\text{rel}}, \quad (13f)$$

where X and Y are defined as $X = \epsilon(\frac{c_n}{m} - \lambda_1)$, $Y = -\frac{c_n}{m}$, and where $V_t = V_x \cos \theta + V_y \sin \theta$ is the current component tangential to the body frame.

Remark 1: Note that the absolute velocities have been replaced by the relative velocities in the model equations.

IV. INTEGRAL LOS PATH FOLLOWING CONTROL

This section summarizes the integral line-of-sight path following control schemes for underwater snake robots that were previously presented in [18] and [17] for the complex model and the control-oriented mode, respectively. The controller consists of i) the gait pattern controller, which produces a sinusoidal motion pattern which propels the robot forward, ii) the heading controller, which steers the robot towards and subsequently along the desired path, and iii) the integral LOS guidance law, which generates the desired heading angle in order to follow the desired path. An inner loop PD controller is used to control the joint angles or the joint coordinates ϕ , while an outer loop controller is used for generating the reference joint angles or joint coordinates in order to achieve the desired sinusoidal gait pattern and also the desired heading θ_{ref} (Fig. 2). The waypoint guidance control approach for USRs proposed in Section V is based on the controllers described in this section.

A. Control Objective

The path following control objective is to make the robot converge to the desired straight line path and subsequently progress along the path at some nonzero forward velocity,

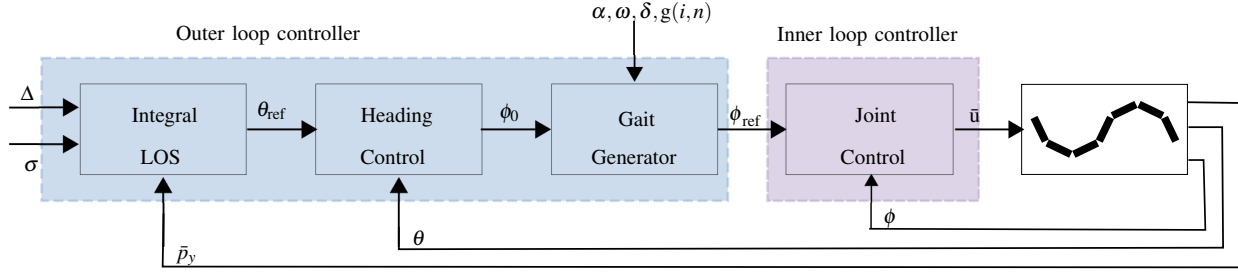


Fig. 2: The structure of the control system

$v_{t,rel} > 0$. Without loss of generality, the global x -axis is aligned with the desired path \mathcal{P} , and thus the position of the robot along the global y axis corresponds to the cross track error, \bar{p}_y . Hence, the control problem is to design a feedback control law for $\bar{\mathbf{u}} \in \mathbb{R}^{n-1}$ such that the following control objectives are achieved:

$$\lim_{t \rightarrow \infty} \bar{p}_y = 0 \quad (14)$$

$$\lim_{t \rightarrow \infty} \theta = \theta_{ss} \quad (15)$$

where θ_{ss} is a constant value which is not required to converge to zero but rather to a steady-state constant value in the presence of ocean currents in the transverse direction of the path. As it is shown in [18], a non-zero angle will allow the underwater snake robot to side-slip in order to compensate for the current effects and thus stay on the desired path.

Remark 2: The relative forward velocity $v_{t,rel}$ is not controlled. By [17] the sinusoidal motion pattern presented in Section IV.B will produce a positive forward velocity, and $v_{t,rel}$ is thus treated as a positive parameter.

B. Motion Pattern

As shown in [18], a general sinusoidal motion pattern can be achieved by making each joint $i \in \{1, \dots, n-1\}$ of the underwater snake robot track the sinusoidal reference signal

$$\phi_i^*(t) = \alpha g(i, n) \sin(\omega t + (i-1)\delta) + \phi_0, \quad (16)$$

where α is the maximum amplitude, ω the frequency, δ the phase shift between the joints, and ϕ_0 is a joint offset that induces turning motion [13], [14]. The function $g(i, n)$ is a scaling function for the joint amplitude along the body. It allows (16) to describe a quite general class of sinusoidal functions. For instance, the choice $g(i, n) = 1$ gives lateral undulation, and $g(i, n) = (n-i)/(n+1)$ gives eel-like motion.

C. Outer-Loop Controller

It is a common approach to choose fixed values for the parameters α and δ for snake-like robots and use the parameters ω, ϕ_0 to control the speed and the direction of the snake robot [13], [14], [18]. In this paper, the same idea will be used in order to steer the underwater snake robot to a desired orientation. Motivated by [22], [23], in [18] the integral LOS method was proposed for USRs where the integral action was added to compensate for the disturbances

by the ocean current. As it was shown in [18], the desired orientation for the USR is given by

$$\theta_{ref} = -\arctan\left(\frac{\bar{p}_y + \sigma y_{int}}{\Delta}\right), \quad \Delta > 0 \quad (17)$$

$$\dot{y}_{int} = \frac{\Delta \dot{\bar{p}}_y}{(\bar{p}_y + \sigma y_{int})^2 + \Delta^2} \quad (18)$$

where Δ (*look-ahead distance*) and $\sigma > 0$ (*integral gain*) are both constant design parameters and the state y_{int} provides the integral action of the guidance law. Please see [18] for more details.

As we have already mentioned, the parameter ϕ_0 will be used to control the direction (heading) of the locomotion of the robot. In [17], based on the control-oriented model presented in Section III, a model-based heading controller that exponentially stabilises the heading of the robot towards the desired heading, was proposed. In particular, it was shown that in order to steer the heading according to the integral LOS angle in (17,18), the joint offset should be defined as

$$\phi_0 = \frac{1}{\lambda_2 v_{t,rel}} \left[\ddot{\theta}_{ref} + \tilde{\lambda}_1 \dot{\theta}_{ref} - k_\theta (\theta - \theta_{ref}) - \frac{\tilde{\lambda}_2}{n-1} v_{t,rel} \sum_{i=1}^{n-1} \alpha g(i) \sin(\omega t + (i-1)\delta) \right], \quad (19)$$

where $k_\theta > 0$ is a control gain. See [17] for more details regarding the derivation of the proposed heading control approach and the stability proof.

Furthermore, based on the complex model presented in Section II, it was shown in [18] that the following simple heading controller is able to steer the heading according to the integral LOS angle in (17,18)

$$\phi_0 = k_\theta (\theta - \theta_{ref}). \quad (20)$$

Note that a formal stability proof for the complex model is not obtained yet due to the complexity of this model. However, extensive simulation results and experimental results presented in [18] and [19], respectively, show that the robot is able to compensate for the ocean current effects and follow the path by using the heading controller given in (20). In this paper, the waypoint guidance proposed in Section V will be implemented considering both (19) and (20) for the directional control of USRs.

D. Inner-loop controller

In order to make the joint angle ϕ_i follow its reference signal ϕ_i^* given by (16), a PD controller is used:

$$\bar{u}_i = k_p(\phi_i^* - \phi_i) + k_d(\dot{\phi}_i^* - \dot{\phi}_i), \quad i = 1, \dots, n-1, \quad (21)$$

where $k_p > 0$ and $k_d > 0$ are the gains of the controller. Note that in [17] it was shown that the joint coordinates exponentially track the reference coordinates given by (16).

V. WAYPOINT GUIDANCE UNDER INFLUENCE OF CURRENT EFFECTS

Nowadays, autonomous underwater vehicles (AUVs) and remotely operated vehicles (ROVs) are widely used in the subsea environment for different challenging tasks [12]. Swimming snake robots represent an interesting alternative to conventional ROVs and AUVs. Inspired by the versatility of biological snake locomotion, snake-like robots carry the potential to meet the growing need for robustness and agility and thus provide new technology that can increase autonomy even in challenging environments. In order to be applicable in such tasks, it is required that the robot can steer itself to one or several specific target location(s). Waypoint guidance is a popular strategy in the field of autonomous underwater vehicles [12]. WPG between the start and end point of a path, $[x_d(t_o), y_d(t_o)]$ and $[x_d(t_f), y_d(t_f)]$, is achieved by splitting the path into a number of waypoints $[x_d(k), y_d(k)]$ for $k = 1, 2, \dots, N_w$, where N_w is the number of waypoints, in between the start and end point. The WPG system switches to the next waypoint when the USR reaches the current one, i.e. when it enters the region of acceptance r_{accept} of the current waypoint $[x_d(k), y_d(k)]$ ([12], [24]). In [24], WPG for land-based snake robots was proposed. Based on this approach, [15] presented a WPG strategy for USRs for obstacle avoidance purposes. In [15], the disturbances due to ocean currents were disregarded. In this paper, the WPG strategy presented in [15] is extended in order to consider general motion control of USRs under the influence of ocean current effects. In particular, in this paper we state the proposed WPG strategy for USRs as follows:

Input : Choose the initial position of the USR

repeat

 Transfer the origin of the global frame to WP k ;

 Orient the global x -axis towards WP $k + 1$;

 Start a path following controller;

if $[p_x, p_y]^T \in r_{accept}$ **then**

 | $k = k + 1$

end

until $k = N_w - 1$;

Algorithm 1: WPG for USRs exposed to ocean current

Simulation results will be presented in the following section to show that the operator-friendly waypoint guidance strategy can be applied independently of the model of the robot and the chosen heading controller approach.

VI. SIMULATION STUDY

This section presents simulation results in order to investigate the performance of the WPG strategy for USRs under the influence of ocean current effects proposed in Section V. In particular, we will present simulation results both for the complex model presented in Section II and the control-oriented model presented in Section III. The dynamic models presented in Section II and Section III were implemented in

Matlab R2013b. The time evolution was calculated using the *ode23tb* solver with a relative and absolute error tolerance of 10^{-4} .

A. Implementation of the Guidance Strategy with the Control-Oriented Model

The USR was considered to consist of $n = 10$ links. The model parameters were chosen in accordance with the parameters of the physical snake robot Mamba [3]: the length of each link was $L = 0.18$ m, the mass $m = 0.8$ kg, the drag parameters $c_n = 17.3, c_t = 4.45$, and the propulsion coefficient $c_p = 35.69$. The rotation parameters were determined as $\tilde{\lambda}_1 = 6, \tilde{\lambda}_2 = 120$ in [8]. From these values, the distance ε was computed. The robot was assumed to face a constant irrotational ocean current $v_c = [-0.07 \ 0.07]^T$ m/s. The parameters for the gait (16) were chosen as $\alpha = 0.07$ m for lateral undulation, $\alpha = 0.1172$ m for eel-like motion, $\omega = 210^\circ/\text{s}$, $\delta = 40^\circ$, and the scaling function as $g(i, n) = 1$ for lateral undulation and $g(i, n) = (n - i)/(n + 1)$ for eel-like motion.

The radius of acceptance for each waypoint was set to $r_{accept} = 0.8$ m and the ILOS path following controller was implemented according to (16) - (19). The gains for the control system were chosen as follows: $k_p = 20$, $k_d = 5$ and $k_\theta = 0.5$. The parameters for the guidance law were set to $\Delta = Ln$ and $\sigma = 0.02 \frac{\text{m}}{\text{s}}$.

In order to obtain the time derivatives of ϕ_0 and θ_{ref} that are required for the controller, third-order low-pass filter reference models were implemented. Details on these reference models can be found in Appendix C.2 in [13]. The parameters of the reference models were chosen as $\omega_c = 2\pi, \zeta = 1$. In addition, the joint angle offset ϕ_0 was saturated at $\phi_0 = [-\alpha, \alpha]$ in order to keep the reference signal within realistic bounds.

The initial configuration of the robot was the following: $\bar{p}_x = 0, \bar{p}_y = 1$ m, $\theta = 0^\circ$, and $\phi = 0$. All initial velocities were set to zero.

B. Implementation of the Guidance Strategy with the Complex Model

The hydrodynamic related parameters $c_t, c_n, \mu_n, \lambda_1, \lambda_2$, and λ_3 were computed for the elliptic link section with major and minor diameters $2a = 2 \cdot 0.055$ m and $2b = 2 \cdot 0.05$ m, respectively. The fluid properties were assumed to be $\rho = 1000 \text{ kg/m}^3$ and $C_f = 0.03, C_D = 1.75, C_A = 1.5, C_M = 1$ and used to compute the parameters by using equations derived in [4]. Note that we consider different values for the fluid parameters of the complex model and the control-oriented model since the control-oriented model considers only the linear drag effects compared to the complex model where both linear and nonlinear drag and added mass effects are taken into account. The orientation of the robot ($\theta = \bar{\theta}$) is calculated as the average of all link angles as given in (1). In addition, the cross-track error for the complex model was set to $\bar{p}_y = p_y$.

The amplitude of the sinusoidal motion pattern was set to $\alpha = 16.72^\circ$ and $\alpha = 30^\circ$ for lateral undulation and eel-like motion, respectively. Note that these values for the

amplitudes of the sinusoidal motion were chosen with respect to the relationship derived in [21] that correlates the amplitude of the complex and the control-oriented model. For the complex model, the ILOS path following controller was implemented according to (16), (17), (18), and (20) with $\Delta = Ln/2$, $\sigma = 0.002 \frac{m}{s}$, and control the gain $k_\theta = 0.5$. Note that the heading controllers (20) and (19) are tuned with different parameters Δ and σ . This is reasonable since they are derived based on two different modeling approaches. Furthermore, the joint angle offset was saturated according to $\phi_0 = [-25^\circ, 25^\circ]$. The remaining parameters were set equal to the parameters presented in Section VI.A.

C. Simulation Results

The efficacy of the waypoint guidance strategy was examined through two different simulation studies. In particular, we performed simulations for the ILOS path following control approaches based on the complex and the control-oriented model presented in Section IV. The desired path was defined by interconnecting the following set of predefined waypoints in the global frame: (0,0), (10,0), (30,0), (40,20), (30,40), (10,40), (0,20) and (10,0). The heading controller was calculated by (19) and (20) for the control-oriented model and the complex model, respectively. Fig. 3 and Fig. 4 show the motion of the CM of the robot for lateral undulation and eel-like motion, respectively. In both cases we see that the USR manages to follow, with almost zero error, the desired path while being able to pass all the defined target points (waypoints).

Furthermore, we see in Fig. 5a and Fig. 5b that the heading controllers given in (19) and (20) combined with (16) make the actual heading angles converge to the desired heading angle given by (17,18) for lateral undulation. Similarly for eel-like motion, Fig. 6a and Fig. 6b show that the heading controllers given in (19) and (20) together with (16) enable the robot to reach the desired heading angle given by (17,18). As it is shown in Fig. 5 and Fig. 6, the heading of the robot does not converge to zero but rather converges to a steady state constant value θ_{ss} , as it is designed to. In particular, the USR keeps a nonzero heading angle in steady state in order to compensate for the current effect. Note that a nonzero angle is what allows the robot to side-slip in order to compensate for the current effects and thus stay on the desired path. In addition, we see from these figures that the steady state angle has different values for different sections of the desired path and this was expected since the ocean current is constant in the global frame and thus the ocean current values in the body frame differ depending on the orientation of the reference straight line section with respect to the global frame. Note that the heading of the snake keeps oscillating about θ_{ss} for the complex model in Fig. 5b and 6b, even in steady state. This is the natural behaviour of a snake-like mechanism. The plots of the control-oriented model in Fig. 5a and Fig. 6a on the other hand do not display such behaviour because the high order oscillations are not captured by the simplified modelling approach.

VII. CONCLUSIONS

In this paper, a waypoint guidance strategy has been presented for steering an underwater snake robot, compensating for ocean current effects along a desired path defined by a set of waypoints interconnected by straight lines. The guidance strategy was built on two different straight line path following control approaches previously proposed by the authors: 1) an ILOS path following controller derived based on a complex model for USRs for which the stability analysis was studied using a Poincaré map, and 2) a model-based control approach derived based on a control-oriented model for USRs. Furthermore, it was shown that the waypoint guidance control strategy using the integral LOS guidance law combined with a directional controller can be applied to USRs to compensate for the ocean current effect and achieve path following along the interconnected straight lines defined by the way points. Simulation results illustrated the performance of the proposed control strategy for both lateral undulation and eel-like motion patterns. In future work, the efficacy of the proposed waypoint guidance strategy will be experimentally investigated using the underwater snake robot Mamba.

REFERENCES

- [1] A. Crespi and A. J. Ijspeert, "AmphiBot II: An Amphibious Snake Robot that Crawls and Swims using a Central Pattern Generator," in *Proc. 9th International Conference on Climbing and Walking Robots (CLAWAR)*, Brussels, Belgium, Sept. 2006, pp. 19–27.
- [2] H. Yamada, S. Chigisaki, M. Mori, K. Takita, K. Ogami, and S. Hirose, "Development of amphibious snake-like robot ACM-R5," in *Proc. 36th International Symposium on Robotics*, Tokyo, Japan, 2005.
- [3] P. Liljebäck, Ø. Stavdahl, K. Pettersen, and J. Gravidahl, "Mamba - a waterproof snake robot with tactile sensing," in *Proc. International Conference on Intelligent Robots and Systems (IROS)*, Chicago, IL, Sept. 14-18 2014, pp. 294–301.
- [4] E. Kelasidi, K. Y. Pettersen, J. T. Gravidahl, and P. Liljebäck, "Modeling of underwater snake robots," in *Proc. IEEE International Conference on Robotics and Automation (ICRA)*, Hong Kong, China, May 31-June 7 2014, pp. 4540–4547.
- [5] K. Melsaac and J. Ostrowski, "A geometric approach to anguilliform locomotion: modelling of an underwater eel robot," in *Proc. International Conference on Robotics and Automation (ICRA)*, vol. 4, Detroit, MI, May 10-15 1999, pp. 2843–2848.
- [6] A. Wiens and M. Nahon, "Optimally efficient swimming in hyper-redundant mechanisms: control, design, and energy recovery," *Bioinspiration & Biomimetics*, vol. 7, no. 4, p. 046016, 2012.
- [7] M. Porez, F. Boyer, and A. J. Ijspeert, "Improved lighthill fish swimming model for bio-inspired robots: Modeling, computational aspects and experimental comparisons," *The International Journal of Robotics Research*, vol. 33, no. 10, pp. 1322–1341, 2014.
- [8] A. M. Kohl, K. Y. Pettersen, E. Kelasidi, and J. T. Gravidahl, "Analysis of underwater snake robot locomotion based on a control-oriented model," in *Proc. IEEE Int. Conf. Robotics and Biomimetics*, Zhuhai, China, Dec. 2015, pp. 1930–1937.
- [9] K. McIsaac and J. Ostrowski, "Motion planning for anguilliform locomotion," *IEEE Transactions on Robotics and Automation*, vol. 19, no. 4, pp. 637–625, 2003.
- [10] L. Lapierre and B. Jouvencel, "Path following control for an eel-like robot," in *Proc. MTS/IEEE International Conference Oceans*, vol. 1, Brest, France, June 20-23 2005, pp. 460–465.
- [11] K. Morgansen, B. Triplett, and D. Klein, "Geometric methods for modeling and control of free-swimming fin-actuated underwater vehicles," *IEEE Transactions on Robotics*, vol. 23, no. 6, pp. 1184–1199, 2007.
- [12] T. I. Fossen, *Handbook of Marine Craft Hydrodynamics and Motion Control*. John Wiley & Sons, Ltd, 2011.
- [13] P. Liljebäck, K. Y. Pettersen, Ø. Stavdahl, and J. T. Gravidahl, *Snake Robots: Modelling, Mechatronics, and Control*. Springer-Verlag, Advances in Industrial Control, 2013.

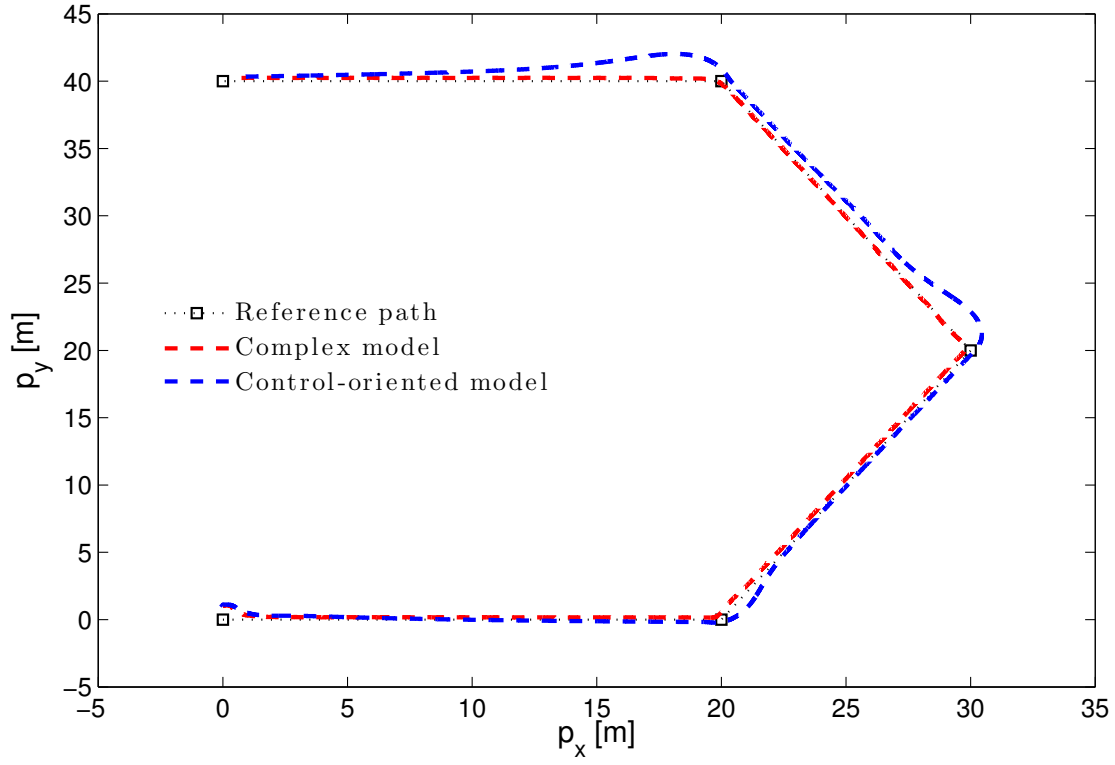


Fig. 3: Path for the lateral undulation motion pattern.

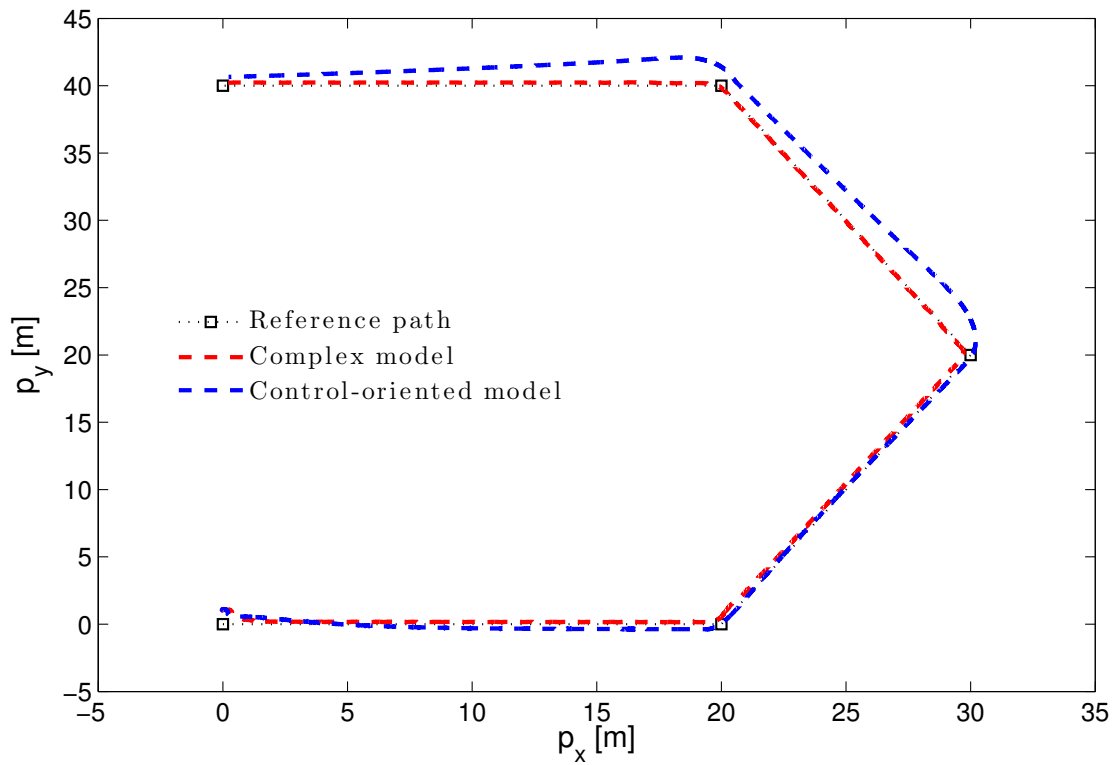
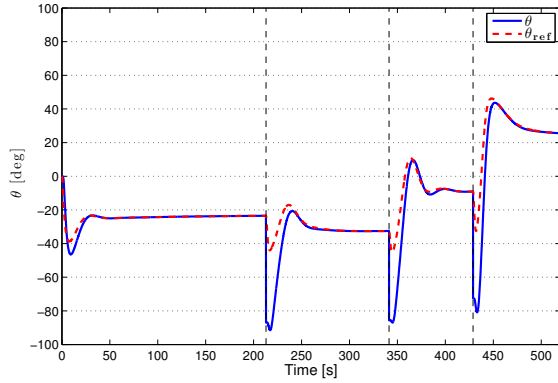
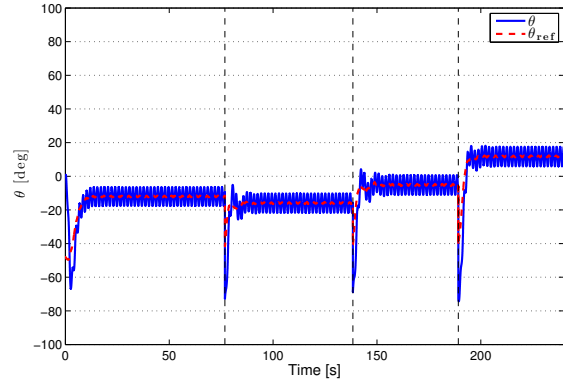


Fig. 4: Path for the eel-like motion pattern.

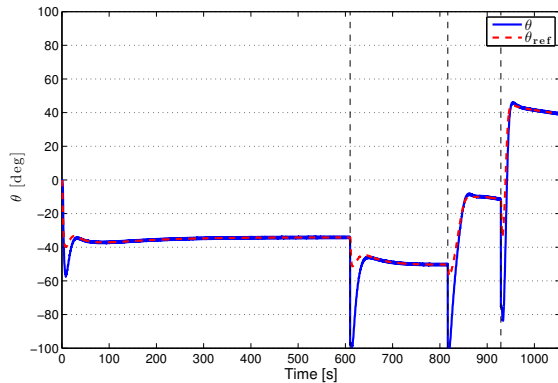


(a) Heading control-oriented model.

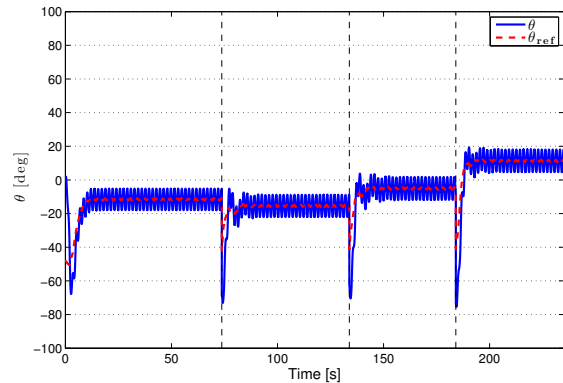


(b) Heading complex model.

Fig. 5: Results for the underwater snake robot for lateral undulation motion pattern.



(a) Heading control-oriented model.



(b) Heading complex model.

Fig. 6: Results for the underwater snake robot for eel-like motion pattern.

- [14] J. Guo, "A waypoint-tracking controller for a biomimetic autonomous underwater vehicle," *Ocean Engineering*, vol. 33, no. 17-18, pp. 2369 – 2380, 2006.
- [15] E. Kelasidi, K. Y. Pettersen, and J. T. Gravdahl, "A waypoint guidance strategy for underwater snake robots," in *Proc. IEEE 22nd Mediterranean Conference on Control and Automation*, Palermo, Italy, June 16-19 2014, pp. 1512–1519.
- [16] M. Kruusmaa, P. Fiorini, W. Megill, M. De Vittorio, O. Akanyeti, F. Visentin, L. Chambers, H. El Daou, M.-C. Fiazza, J. Jezov, M. Listak, L. Rossi, T. Salumae, G. Toming, R. Venturelli, D. Jung, J. Brown, F. Rizzi, A. Quattieri, J. Maud, and A. Liszewski, "Filose for svenning: A flow sensing bioinspired robot," *IEEE Robotics Automation Magazine*, vol. 21, no. 3, pp. 51–62, 2014.
- [17] A. M. Kohl, K. Y. Pettersen, E. Kelasidi, and J. T. Gravdahl, "Planar path following of underwater snake robots in the presence of ocean currents," *IEEE Robotics and Automation Letters*, vol. 1, no. 1, pp. 383–390, 2016.
- [18] E. Kelasidi, K. Y. Pettersen, P. Liljebäck, and J. T. Gravdahl, "Integral line-of-sight for path-following of underwater snake robots," in *Proc. IEEE Multi-Conference on Systems and Control*, Juan Les Antibes, France, Oct. 8-10 2014, pp. 1078 – 1085.
- [19] E. Kelasidi, P. Liljebäck, K. Y. Pettersen, and J. T. Gravdahl, "Integral line-of-sight guidance for path following control of underwater snake robots: Theory and experiments," in *IEEE Transactions on Robotics*, 2014, (Submitted).
- [20] E. Kelasidi, K. Y. Pettersen, and J. T. Gravdahl, "A control-oriented model of underwater snake robots," in *Proc. IEEE International Conference on Robotics and Biomimetics (ROBIO)*, Bali, Indonesia, Dec. 5-10 2014, pp. 753–760.
- [21] A. M. Kohl, E. Kelasidi, K. Y. Pettersen, and J. T. Gravdahl, "A control-oriented model of underwater snake robots exposed to currents," in *Proc. IEEE Multi-Conference on Systems and Control*, Sydney, Australia, Sep. 21-23 2015, pp. 1585 – 1592.
- [22] E. Borhaug, A. Pavlov, and K. Pettersen, "Integral LOS control for path following of underactuated marine surface vessels in the presence of constant ocean currents," in *Proc. 47th IEEE Conference on Decision and Control (CDC)*, Cancun, Dec. 9-11 2008, pp. 4984–4991.
- [23] W. Caharija, K. Pettersen, A. Sorensen, M. Candeloro, and J. Gravdahl, "Relative velocity control and integral line of sight for path following of autonomous surface vessels: Merging intuition with theory," *Part M: Journal of Engineering for the Maritime Environment*, vol. 228, no. 2, pp. 180–191, 2013.
- [24] P. Liljebäck and K. Y. Pettersen, "Waypoint guidance control of snake robots," in *Proc. IEEE International Conference on Robotics and Automation (ICRA)*, Shanghai, China, May 9-13 2011, pp. 937–944.